Journal of Magnetic Resonance 209 (2011) 315–322

Contents lists available at ScienceDirect

Journal of Magnetic Resonance

journal homepage: www.elsevier.com/locate/jmr

Spin–spin coupling edition in chiral liquid crystal NMR solvent

Denis Merlet, Laetitia Béguin, Jacques Courtieu, Nicolas Giraud *

Equipe de RMN en milieu orienté, ICMMO, UMR 8182 CNRS Univ Paris-Sud 11, bât 410, 91405 Orsay cedex, France

ARTICLE INFO

Article history:
Received 4 November 2010
Revised 17 January 2011
Available online 3 February 2011

Keywords:
Nuclear magnetic resonance
J (T)-resolved spectrum
SERFph experiment
G-SERF experiment
Pulsed field gradient
Frequency sweep
Spatial frequency encoding
Parallel acquisition
Enantiomeric discrimination
Residual dipolar couplings
Chirality
PBLG

ABSTRACT

The application of the G-SERFph pulse sequence is presented on enantiomeric mixtures dissolved in a chiral liquid crystal. It aims at editing, within one single 2D spectrum, every proton coupling which is experienced by a given proton site in the molecule, and leads to *real* phased *T*-edited spectroscopy ($T = J + 2D$). This NMR experiment is based on the combination of homonuclear semi-selective refocusing techniques with a spatial *frequency* encoding of the sample. This approach, which consists in handling selectively each coupling in separate cross sections of the sample, is applied to the visualization of enantiomers dissolved in a chiral liquid crystalline phase. Advantages and limits of this methodology are widely discussed.

1. Introduction

Gradient encoded spectroscopy [1–9] has recently aroused a great interest in very different fields of Nuclear Magnetic Resonance. The implementation of radiofrequency (*r.f.*) fields that are applied simultaneously to pulsed field gradients has led to a wide range of achievements as diverse as the recording of *single scan* multi-dimensional experiments, or *J*-resolved spectroscopy [1,6,8,10] ... The methodology behind these applications can be divided in two groups. In the first of them, the combination of frequency swept pulses with a field gradient results in the acquisition of different evolution periods τ for molecules which are in different parts of the sample [3,7]. This irradiation scheme, which creates a spatial *time* encoding of the whole spectrum throughout the sample, represents a good alternative to other analogous encoding techniques, in sofar as it allows for a significant simplification of the pulse sequences. It constitutes now the basis for Ultrafast (or *single scan*) NMR spectroscopy [7]. Spatial time encoding techniques have also been used for more specific purposes, such as implementing Zero Quantum filters [2], or running different INEPT transfers at the same time, which is the cornerstone of QQ-HSQC experiments.[5] This latter experiment derives from the parallel acquisition approach [11,12].

The second group is referred to as spatial *frequency* encoding. It is based on the use of semi-selective pulses [13], still in the presence of a field gradient, which allow to handle *different* spin coherences in *different* parts of the sample. This methodology has also generated considerable developments in the field of parallel acquisition experiments. It has been used for instance to acquire broadband homodecoupled ^{1}H spectra [14]. More recently, we have presented the Gradient encoded homonuclear SElective ReFocusing experiment (G-SERF), which originates from this latter approach: a spatial *frequency* encoding is created along the sample, which allows to select, in separate cross sections, each interaction which is involved in the coupling network around a given proton site. On the resulting 2D spectrum, each coupling can be straightforwardly assigned and measured, on a fully resolved multiplet, at the resonance frequency of the coupling partner [15]. The great simplification of *pure J*-resolved spectra which are acquired using this approach, potentially paves the way for the investigation of more complex spin networks.

A particularly challenging case is the visualization of enantiomers which are dissolved in a weakly orienting chiral liquid crystal solvent [16]. In this kind of anisotropic medium, intermolecular interactions in the spin Hamiltonian are averaged to zero by translational and rotational diffusion of the molecules in the mesophase, whereas there is only a partial averaging of intramolecular spin interactions [17]. The magnitudes of these partially-averaged interactions depend on the orientational order of the molecules

* Corresponding author. Fax: +33 1 69 15 81 05.
E-mail address: nicolas.giraud@u-psud.fr (N. Giraud).

1090-7807/$ - see front matter © 2011 Elsevier Inc. All rights reserved.
doi:10.1016/j.jmr.2011.01.030

in the liquid crystalline phase [18]. Furthermore, in a chiral anisotropic solvent, enantiomers do not have the same orientational order [19,20]. Consequently, all the order-dependent NMR interactions, namely the chemical shift anisotropy, the residual dipolar coupling or the quadrupolar splitting, will be different for each isomer. In other words, NMR spectra of enantiomers dissolved in a chiral liquid crystal are different. Among all the chiral liquid crystals which can be used as an NMR solvent for chiral discrimination, lyotropic phases made of poly-γ-benzyl-L-glutamate (PBLG), dissolved in chloroform or DMF, constitute probably the most commonly used oriented medium (other chiral anisotropic NMR solvents can also be found in the literature [21–23]).

Similarly to other anisotropic systems, where proton spins are connected together by a dipolar network, solutes dissolved in PBLG/organic solvent usually show proton spectra that are too complex to be useful as such [24]. It should be noted that proton spectroscopy is 10^6 times more sensitive than deuterium which has provided the first simple spectral discrimination at natural abundance. However, methods had to be sought to enhance the resolution in these proton spectra. Indeed, in a PBLG phase, the proton spectrum is often composed of broad multiplets: although several ^{1}H NMR experiments have been recently developed in that field, the resulting signals still need to be resolved [25–28]. In this context, Béguin et al. have recently shown that SElective ReFocusing (SERF) experiments allow to dramatically reduce the number of interactions that contribute to proton lineshape in PBLG/$CDCl_3$ solvent, and lead to the observation, for each enantiomer, of a single proton-proton overall coupling T ($T = J + 2D$, with J and D being the scalar and dipolar coupling, respectively) [29].

In this paper, we present the application of the (phaseable) G-SERFph experiment to a chiral compound dissolved in a PBLG/$CDCl_3$ chiral solvent. We demonstrate that an enantiomeric visualization can be achieved easily, for a given proton site, through the whole dipolar network around it, with a single 2D spectrum. We also evaluate the robustness of this pulse sequence when it is used to probe fully coupled systems, through (i) an analysis of the experimental artifacts that may be generated, and (ii) a comparison to analogous data that are yielded by a SERFph pulse sequence which has given the best resolved data so far [30]. Finally, we discuss the advantages and drawbacks of this methodology, regarding the great number of structural constraints which have to be collected in dipolar coupled proton systems, when the size of the spin network increases.

2. Results and discussion

2.1. Sample preparation and spatial frequency encoding calibration

Propylene oxide (Fig. 1a) was chosen as a chiral model organic compound in order to illustrate the properties of the G-SERFph pulse sequence on molecules dissolved in a chiral liquid crystalline phase. The NMR sample was obtained by diluting 55 mg of a mixture of propylene oxide (enantiomeric excess in *R*: 25%) in a liquid-crystalline phase composed of 100 mg of poly-(γ-benzyl)-L-glutamate (PBLG, purchased from Sigma, D.P. = 782) and 677 mg of $CDCl_3$, using standard procedure described elsewhere [31]. The resulting 5 mm NMR tube was then sealed in order to avoid solvent evaporation, and centrifuged back and forth until an optically homogeneous birefringent phase was obtained.

All the NMR experiments were carried out on a 14.1 T Bruker Avance II spectrometer, using a 5 mm ^{2}H/^{1}H cryogenically cooled probe equipped with a *z* field gradient coil. The probe temperature was set to 304 K. A preliminary calibration of the spatial frequency encoding was performed, in order to select the volume from the sample along which the proton spectrum is encoded. This step,

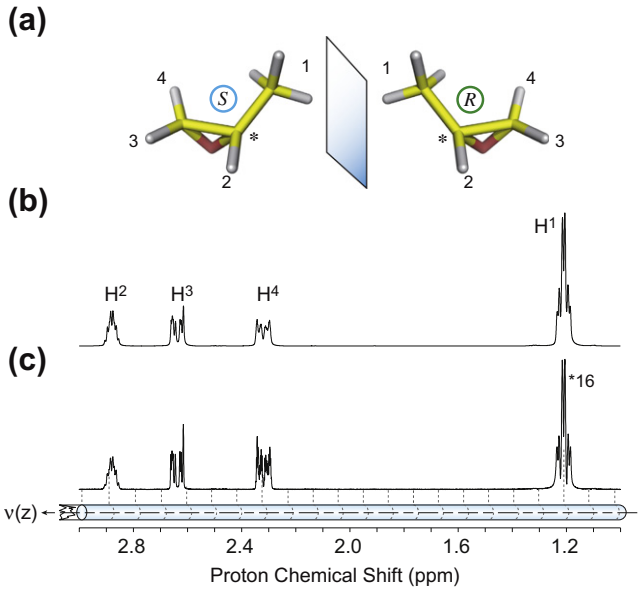

Fig. 1. (a) The structure and atomic labeling of both enantiomers of propylene oxide (1,2-epoxypropane). Covalent bonds are displayed as sticks which are coloured in yellow (resp. white or red) around carbon atoms (resp. proton, oxygen atoms). (b) The broadband excitation spectrum, recorded on propylene oxide dissolved in PBLG, and (c) the proton spectrum which was acquired using a semi-selective Gaussian pulse (of duration 20 ms – the nutation angle of this excitation pulse was set to 270°), applied together with a rectangular *z* pulsed field gradient of 0.2 G/cm strength. An NMR tube is drawn along the spectrum, in order to illustrate the spatial *frequency* encoding of proton lines according to their resonance frequencies. (For interpretation of the references to colour in this figure legend, the reader is referred to the web version of this article.)

which depends on both the strength of the encoding field gradient, and the selectivity of the *r.f.* field, is of particular importance for anisotropic samples, due to the broad lines of their ^{1}H spectra. These parameters, as well as the offset of the soft pulse, were adjusted so that the resulting spectrum has the same intensity profile as a reference broadband excitation spectrum (shown in Fig. 1-b).

Fig. 1c shows a typical encoded ^{1}H spectrum which was recorded at the end of the calibration step of the spatial frequency encoding. As it was already described [15,32], slightly narrower linewidths can be measured on this spectrum (compared with the standard broadband spectrum presented above), due to the fact that each line comes from a restricted volume of the sample.

2.2. ^{1}H G-SERFph 2D spectrum

Fig. 2 shows the 2D spectrum which was recorded on propylene oxide dissolved in the PBLG/$CDCl_3$ solvent, using the G-SERFph pulse sequence. In the refocusing block, the offset of the first and third semi-selective pulses (which are inversion pulses) was set at the H^2 resonance frequency, so as to edit every coupling involving this proton (the detail of the pulse sequence, and notably the protocol for the calibration of the pulses, have been published elsewhere[15]).

The duration of these two non-encoded pulses was determined so that they invert properly the signal from H^2 (i.e. the proton spin whose couplings are being edited on this spectrum). The gradient-encoded refocusing pulse was calibrated through a direct optimization of the first experiment of the G-SERFph pulse sequence (corresponding to $t_1 = 6$ μs) in order to minimize signal distortions. In particular, we have experimentally determined that the gradient-encoded refocusing pulse had to be longer than the gradient-encoded excitation pulse, in order to observe an efficient refocusing of the interactions (we discuss further which kind of

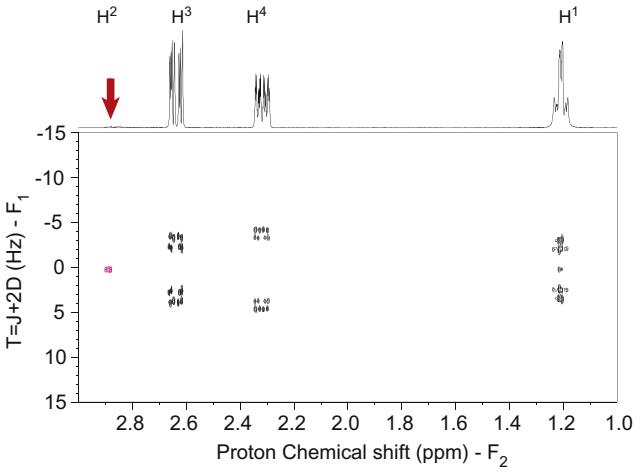

Fig. 2. The G-SERFph proton 2D spectrum which was recorded on propylene oxide dissolved in a chiral liquid crystalline solvent composed of PBLG and $CDCl_3$ (the positive projection of the rows is shown above the spectrum). The signal at H^2 chemical shift (in red) is phased as a negative peak. All the semi-selective pulses have a Gaussian shape. The nutation angle of the excitation pulse was calibrated at 270°. The duration of the initial gradient-encoded excitation pulse (respectively the second gradient-encoded refocusing pulse) was 20 ms (resp. 40 ms). The offset of the non-encoded soft inversion pulse, of duration 6 ms, was set at the resonance frequency of H^2 (red arrow). The sample was frequency encoded by a rectangular *z* pulsed field gradient of 0.2 G/cm strength. Gradient coherence selection was achieved by sine-shaped gradient pulses of 0.75 ms duration and 26 G/cm strength, followed by recovery delays of 0.25 ms. Another sine-shaped gradient of 1.5 ms duration and 42 G/cm strength, followed by a recovery delay of 0.2 ms was used in the *z* gradient filter. A phaseable 2D map was obtained with TPPI. Each of the 768 increments in t_1 were acquired with 8 scans and a 2 s recycle delay between scans, with maximum acquisition times of 3.84 s in t_1 and 2 s in t_2 (corresponding to the acquisition of a free induction decay over 6242 points). Data were processed using zero-filling up to 1024 points in t_1, and 8192 points in t_2, automatic baseline correction in both dimensions and symmetryzation in the indirect domain. This spectrum was recorded in 10.5 h (due to the great number of points acquired during t_1, in order to obtain a high-resolution spectrum in F_1). (For interpretation of the references to colour in this figure legend, the reader is referred to the web version of this article.)

artifacts this experimental setting can give rise to). The *r.f.* field strength of the non-encoded inversion pulses was also adjusted over a direct optimization of a G-SERFph 1D spectrum.

We observe, at H^1 (resp. H^3 and H^4) chemical shift, two doublets whose splittings T_R^{12} and T_S^{12} (resp. $T_{R/S}^{23}$ and $T_{R/S}^{24}$) can be assigned to each enantiomer (Fig. 3a). This spectrum allows the measurement of all the coupling network from the spin H^2 in both enantiomers, as is illustrated in Fig. 3b.

Furthermore, the coupling values which are measured directly on the G-SERFph spectrum allow to fully interpret the analogous multiplet (Fig. 3c) extracted from a classical *J*-resolved experiment [33] recorded on the same sample. This signal contains exactly the same information about the coupling network around H^2, but would have been impossible to assign without additional data.

The same G-SERFph data were recorded with offsets set at H^1, H^3 and H^4 resonance frequencies. The resulting 2D spectra are shown in Fig. 5 (for H^1) and in supplementary data in Fig. S2 (the complete set of multiplets which can be extracted from all the G-SERFph spectra which were recorded on this sample is presented in supplementary data in Fig. S3).

Moreover, two kinds of artifacts are observed on this spectrum (which did not appear when the G-SERF experiment was applied to an isotropic sample under similar experimental conditions [15]). On the one hand, although signals at H^2, H^3 and H^4 resonance frequencies show very weak artifacts, a careful study of the whole series of G-SERFph spectra recorded on this sample (Figs. 2 and 5, and in supplementary data) reveals that the strongest artifacts only appear at the H^1 (methyl protons) resonance frequency. We note here that in an anisotropic solvent, methyl protons have the same chemical shift, but are dipolar coupled to each other, so that they actually constitute a strongly coupled A_3 spin system [34]. On the other hand, another unexpected signal is observed at H^2 resonance frequency (*i.e.* the proton spin whose couplings are being edited in this experiment). A negative singlet is observed, whereas the coherence transfer pathway which has been set should not leave any signal at this chemical shift [15]. In the following, we describe in detail how the G-SERFph sequence deals with (i) any miscalibration of the excitation and/or refocusing soft pulses, and (ii) a difference in selectivity between the different gradient-encoded pulses, in order to explain how unwanted coherence pathways are removed (or not).

2.3. Effect of selection gradients and phase cycling on experimental artifacts

During a gradient encoded homonuclear selective refocusing experiment, two kinds of sequence imperfection need to be taken into account.

Firstly, pulse miscalibration may cause the creation of undesired coherences. In the G-SERFph pulse sequence, the desired coherence transfer pathways are selected by both the phase cycling of the three excitation or flip-back soft pulses (which are independently cycled), and gradient selection: two gradient pulses are applied before and after the first two successive pulses, in the middle of the t_1 delay, in order to select the coherence pathway associated with a perfect refocusing block [15]. We note here that since a selective refocusing is performed within each cross section, selection gradients have to be strong enough to achieve a complete dephasing and rephasing of coherences within these cross sections.

Secondly, we observe that some additional signals, which are more specific to this experiment, arise from the difference in selectivity between the spatially encoded excitation and refocusing pulses. Fig. 4 describes how the magnetization from a given proton spin, whose signal is encoded in a particular region of the sample, interacts with each selective irradiation. Note that the G-SERFph experiment which is simulated in Fig. 4 is set for the edition of H^2's couplings: the results which are presented here for H^4 would lead to the same result if one considered the cross sections where H^1 or H^3 (instead of H^4) are encoded.

The desired signal originates from the magnetization pathway (b): in this cross section, proton spins H^4 are excited by the first, spatially-encoded, excitation pulse. Then, in the refocusing block, the two non-encoded and the spatially encoded pulses act on H^2 and H^4 coherences respectively. During the resulting spin evolution, all the interactions that involve H^4 are refocused, except the H^2–H^4 coupling T^{24}. For first order spin systems however, three different artifacts can appear:

(i) In magnetization pathway (a), proton spins H^4 only undergo a selective excitation pulse. Due to the action of the non-encoded inversion pulses, T^{24} is then refocused, whereas every other interaction is evolving during t_1.
(ii) In magnetization pathway (c), proton spins H^2 are excited by the first spatially encoded pulse, but are not affected by the spatially encoded refocusing pulse. Every interaction which involves H^2 is then refocused by the non-encoded refocusing pulses.
(iii) Conversely, in pathway (d), H^2 spins are affected by the whole sequence of spatially encoded, as well as non-encoded refocusing pulses. No interaction is thus refocused for these proton spins.

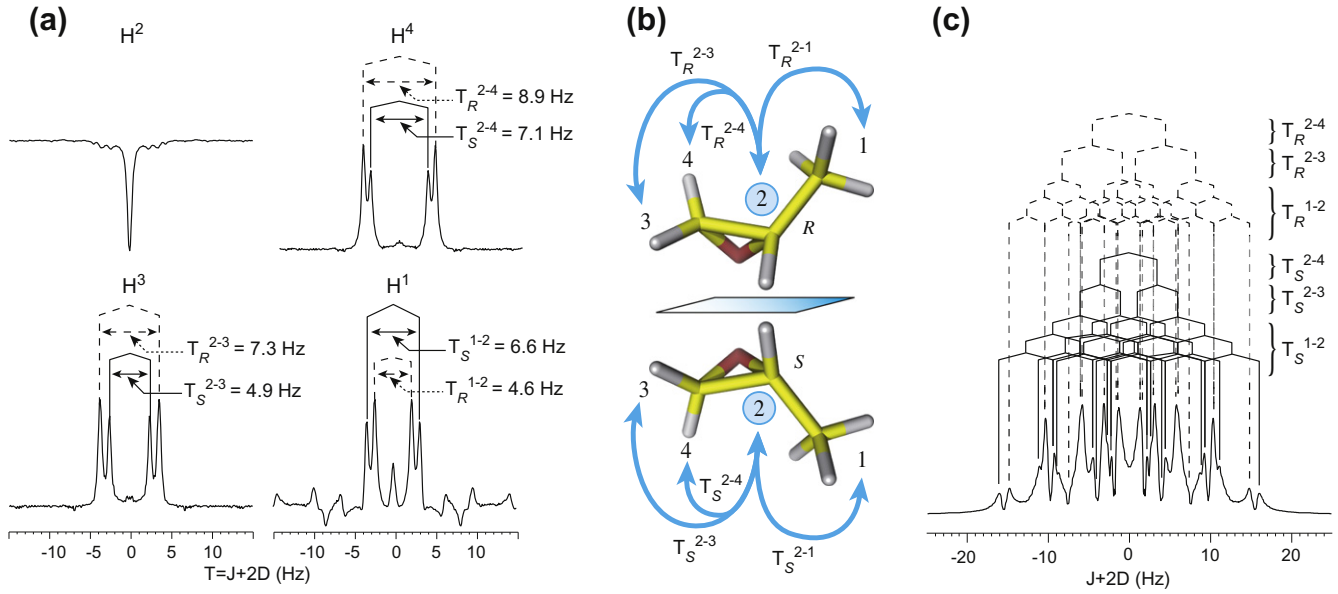

Fig. 3. (a) The sums of the columns (F_1 dimension) taken around the resonance frequencies of the four proton spins in propylene oxide, on the 2D G-SERFph spectrum presented above. (b) The coupling networks which involve the proton spin H^2 in each enantiomer. (c) The F_1 multiplet which was extracted at H^2 chemical shift from a *J*-resolved experiment which was run on the same sample (the whole 2D spectrum, as well as the experimental details are in the supplementary data in Fig. S1).

Sub-signals (a) and (d) do not contribute to the overall spectrum since they are removed by gradient selection. Finally, only the sub-spectra originating from magnetization pathways (b) (which corresponds to the desired evolution of H^4 under T^{24}) and (c) appear on the overall spectrum.

Interestingly, from all the artifacts that could be expected, only the latter can be observed on the spectrum. This analysis indicates that the biggest artifacts, which are observed at H^1 resonance frequency, are actually mainly due to a second-order coupling effect. These signals, which are created by coherence transfers during refocusing pulses, follow the same coherence transfer pathways as the desired signals. Thrippleton et al. have proposed methods that allow to suppress these artifacts, some of them being also based on the use of a frequency sweep during pulses [35]. We note however that second-order systems can provide useful additional information such as the relative sign of the coupling interactions in some spin systems. Nevertheless, the determination and the understanding of the contribution of second-order effects to the lineshape in A_3 spin systems, as well as the experimental suppression of the corresponding artifacts in a G-SERFph experiment, require further simulations and methodological developments which are out of the scope of this paper.

To summarize, most of the artifacts which come from pulse imperfections in the G-SERFph pulse sequence can be removed, for first-order spectra, by standard phase cycling and gradient selection procedures, except a negative singlet which marks the frequency of the proton spin whose couplings are being edited. This latter line does not stop other multiplets from being analyzed, since it does not overlap with any of them. However, as is often the case with chiral oriented media, strongly coupled spin systems contribute to the creation of coherences that cannot be removed by standard coherence selection techniques. Nevertheless, they provide second-order sub-spectra which do not hinder the analysis of the different spin–spin interactions.

2.4. Comparison of SERFph and G-SERFph spectroscopies

In this section, we compare the G-SERFph experiment with the analogous data that can be acquired using our latest development of the SERFph pulse sequence.[30] We have acquired a G-SERFph spectrum which we have set for the edition of the couplings around methyl protons H^1 (Fig. 5a). We have also run, under the same experimental conditions, the series of four SERFph experiments which allows to gather the same collection of correlation spectra (Fig. 5b). Note that since the G-SERFph pulse sequence uses semi-selective irradiations in order to generate a spatial frequency encoding, the *z* gradient filter in both experiments has been implemented with semi-selective flip-back and excitation pulses, whereas the SERFph sequence which is presented by Beguin et al. uses hard pulses [30]. The use of soft pulses presents the advantage of avoiding the creation of zero quantum coherences which would evolve during the *z* gradient filter, and could cause lineshapes distorsions.

For each proton site of the molecule, we observe the same correlation pattern in the G-SERFph and SERFph experiment, except for methyl protons H^1 (the structure of these multiplets is discussed further). We remark that the assignment of the couplings is straightforward with the G-SERFph spectrum (although the identification of each enantiomer is not possible without additional reference data), whereas running a SERFph experiment requires that the coupling partners of a given proton site have already been identified, in order to set the offsets of the soft pulses adequately. The multiplets that can be extracted from the data presented in Fig. 5 are displayed in Fig. 6. At H^2, H^3 and H^4 chemical shifts (Fig. 6a–c), we observe the same multiplet structures in the G-SERFph spectrum as in each related SERFph spectrum. H^2 spin (respectively H^3 and H^4) is coupled to the three methyl protons H^1 and his signal is splitted into a quartet (with intensity ratio 1:3:3:1) for each enantiomer.

Furthermore, we observe that the enantiomeric differentiation is obvious for H^2, but much less easy to probe for H^3, since the couplings T_S^{13} and T_R^{13} are too small to produce measurable splittings. Nevertheless, a thorough analysis of the correlation pattern at H^3 chemical shift (Fig. 7) allows to assign to each enantiomer multiplet structures whose resolution is actually only limited by the proton linewidth (which is about 0.6 Hz for this sample).

Carrying on the multiplet analysis, a single quartet is observed for H^4 spin (Fig. 6c), which means that the overall coupling

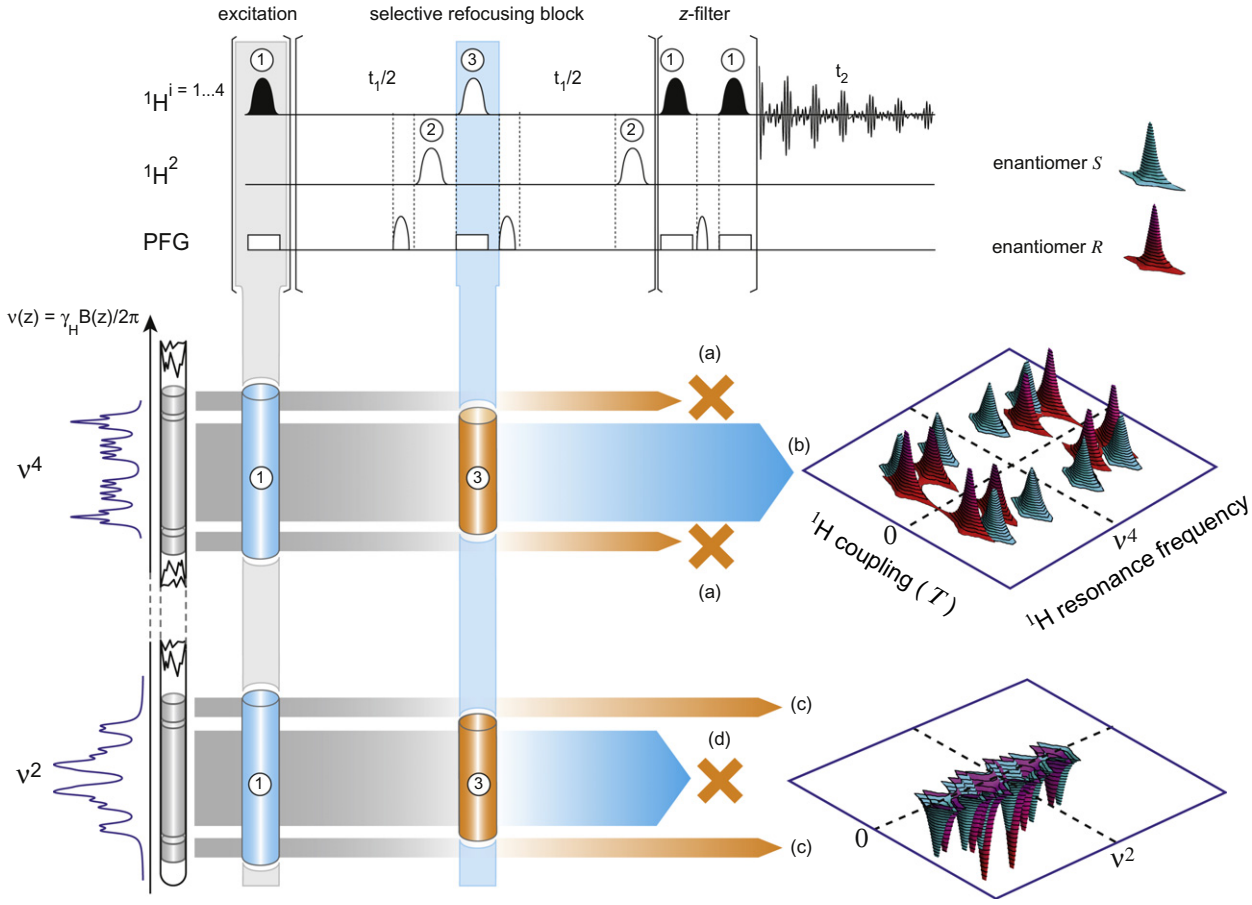

Fig. 4. Schematic representation of the effect of gradient-encoded excitation and refocusing pulses with different selectivities on the resulting spatially encoded signal, in a G-SERFph experiment. The simulated spin system corresponds to the proton network in propylene oxide (proton chemical shift anisotropy is neglected in this simulation). On the proton channels, black and white ellipsoidal shapes correspond respectively to excitation (or flip-back) and refocusing (or inversion) semi-selective shaped pulses. On the pulsed field gradient channel (PFG), white rectangular bars refer to the application of a spatial frequency encoding z field gradient ("rectangular" gradient), and open ellipsoidal shapes to shaped z field gradients used for gradient selection. For the sake of clarity, proton pulses which are not applied simultaneously to a field gradient are depicted on an independent channel ($^1H^2$). The gradient-encoded pulses (1) and (3) do not have the same duration. The widths of the slices which undergo excitation (blue cylinder) or refocusing (orange cylinder) are hence different. Note that the pulses in the z gradient filter have the same selectivity as the initial excitation pulse (1), and do not appear in this analysis for clarity. The offset of the second (non-encoded) inversion pulse (2) is set at H^2 resonance frequency and we assume that no artifact is introduced by this pulse. It is calibrated with respect to the width of H^2's signal, and contributes to the refocusing of spin interactions in the cross section ν^2, as well as in every cross section where a coupling T^{2-i} (i = 1,3,4) involving H^2 is evolving. In the cross section ν^4, proton spins H^4 are first excited by the gradient encoded pulse (1), and their magnetization is modulated during t_1 only by the coupling with H^2, due to the selective refocusing block (note that the same process occurs for the proton spin H^1 and H^3, in the slices ν^1 and ν^3 respectively). A sub-spectrum (b) is obtained, where the splittings T_R^{24} and T_S^{24} can be measured in F_1. Furthermore, due to the different selectivities of the gradient-encoded excitation and refocusing pulses (1) and (3), a fraction of the proton spins H^4 (slice ν^4) do not interact with the gradient-encoded refocusing pulse, while the non-encoded pulses refocus $T_{R/S}^{24}$ evolution. The corresponding sub-signal (a), where H^1 chemical shift and all couplings involving H^1 except $T_{R/S}^{24}$ have evolved during t_1, does not follow the selected coherence pathway. It is then removed by selection gradients (the cancellation of this signal is symbolized by an orange cross). In the cross section ν^2, H^2 spins undergo two successive semi-selective refocusing and inversion pulses: their magnetization evolves under chemical shift interaction (at frequency ν^2), as well as every dipolar and scalar interactions. Finally, the third soft pulse inverts the resulting sub-signal (d) which should appear as a fully coupled multiplet centered at ν^2 resonance frequency in the indirect domain: it is also removed by the two selection gradients. In this cross section however, a part of the proton spins H^2 does not interact with the gradient-encoded refocusing pulse, but only with the non-encoded inversion pulse, which refocuses every interaction (chemical shift, scalar and dipolar couplings). On the resulting spectrum, the sub-signal (c) yields a negative singlet in the middle of the indirect dimension (F_1), and at ν^2 frequency in F_2. (For interpretation of the references to colour in this figure legend, the reader is referred to the web version of this article.)

between H^1 and H^4 is the same for both enantiomers ($T_S^{14} = T_R^{14}$): the enantiomeric differentiation cannot be visualized using this interaction.

Finally, the only differences that are observed between SERFph and G-SERFph correlations involve the protons from the methyl group. On the one hand, in Fig. 6d (above), the SERFph experiment has been set to let evolve only the coupling between the H^1 proton spins. For this strongly coupled A_3 spin system, each proton H^1 interacts during t_1 with the two other spins H^1 of the methyl group, and leads to the observation of two triplets (one per enantiomer), as expected. On the other hand, the structure of the multiplet which is observed on the G-SERFph spectrum (Fig. 6d below), at H^1 resonance frequency, is less intuitive. First, it is negative because the last semi-selective pulse from the refocusing block leads to an inversion of the H^1 signal. Second, its multiplicity corresponds to the addition of two "first-order" triplets (one per enantiomer) and two "second-order" doublets with splittings T_S^{11} and T_R^{11}. We indicate here that since $T_R^{11} \approx 2 \cdot T_S^{11}$, the second order doublet from the R enantiomer overlaps the external lines of the first order triplet from the S enantiomer. We remark here that the analysis of the multiplet that is extracted from the G-SERFph spectrum for the methyl protons H^1 is less obvious, since (i) the values of the couplings T_S^{11} and T_R^{11} lead to a signal overlap, and (ii) this second order spectrum shows a more complex multiplicity as well as a partial distorsion. Nevertheless, even in the case of an A_3 spin system which does not yield exactly the same pattern in

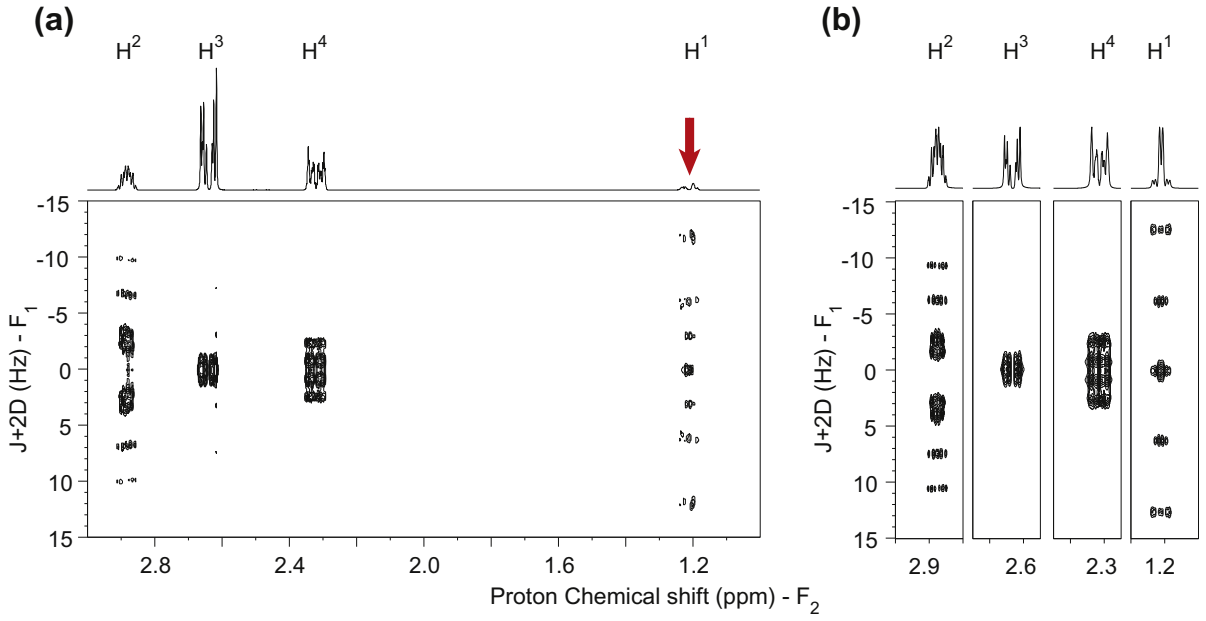

Fig. 5. (a) The G-SERFph proton 2D spectrum recorded on propylene oxide dissolved in PBLG/$CDCl_3$, under the same experimental conditions as the spectrum in Fig. 2. In this experiment, the offset of the non-encoded inversion pulse is set at H^1 resonance frequency (red arrow), in order to edit every coupling which involves the methyl protons. (b) The set of four SERFph experiments which were recorded under similar experimental conditions on the same sample. In each of the first three SERFph experiments, the refocusing pulses were set in order to irradiate H^1 spins on the one hand, and H^2, H^3 or H^4 spins on the other hand, so that multiplets with splittings T^{1-i} (i = 2, 3 or 4) are obtained for each enantiomer at H^2, H^3 or H^4 resonance frequencies respectively. Gaussian pulses of 8 ms were used for the excitation as well as the refocusing pulses. Gradient coherence selection was achieved by sine-shaped gradient pulses of 1.5 ms duration and 10 G/cm strength, followed by recovery delays of 150 μs. Another sine-shaped gradient of 1 ms duration and 5 G/cm strength, followed by a recovery delay of 200 μs was used in the z gradient filter. Phaseable 2D spectra were obtained with Quadrature Sequential Mode. Each of the 768 increments in t_1 was acquired with 4 scans and a 1.5 s recycle delay between scans. The free induction decay was acquired over 6242 points. Data were processed using zero-filling up to 1024 points in t_1, and 8192 points in t_2, automatic baseline correction in both dimensions and symmetrization in the indirect domain. In the last SERFph experiment, the two pulses at $t_1/2$ were replaced with a single refocusing soft pulse at H^1 resonance frequency. Each SERFph spectrum was recorded in 7.5 h. (For interpretation of the references to colour in this figure legend, the reader is referred to the web version of this article.)

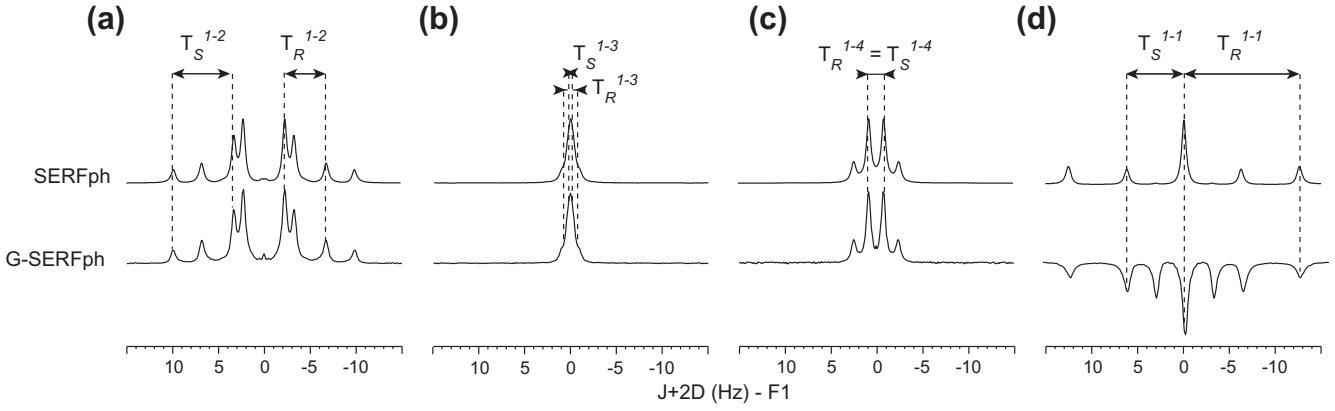

Fig. 6. The sums of the F_1 columns taken around the resonance frequencies of the proton spins (a) H^2, (b) H^3, (c) H^4 and (d) H^1, from the 2D SERFph (above) and G-SERFph (below) spectra which are shown in Fig. 5.

the SERFph or in the G-SERFph experiment, the same couplings can be extracted.

To conclude for this part, the lineshape analysis, on datasets which were acquired using either the SERFph or the G-SERFph approach, shows that the spatial frequency encoding did not introduce any distorsion resulting from uncontrolled spin evolutions during the selective refocusing block. We also observe that the linewidth in the indirect dimension is almost the same in the G-SERFph and in the SERFph spectra (Figs. 6 and 7): we deduce that the spatial encoding does not introduce any relaxation process which could broaden the lines in F_1 dimension. Finally, the same analytical content can be extracted from both kinds of spectra, whose resolution is the same. However, the lower sensitivity which is inherent to the gradient encoding approach may be the only issue that may prevent the G-SERFph experiment from being fully suitable for the analysis of enantiomeric mixtures, in a chiral oriented medium.

2.5. Sensitivity vs experimental time

The G-SERFph experiment is intrinsically less sensitive than a SERFph experiment, because only a spatially-restricted cross section in the sample gives rise to the signal at a given resonance frequency. The loss in sensitivity can be estimated to $\Delta\nu/\gamma.G.l$,

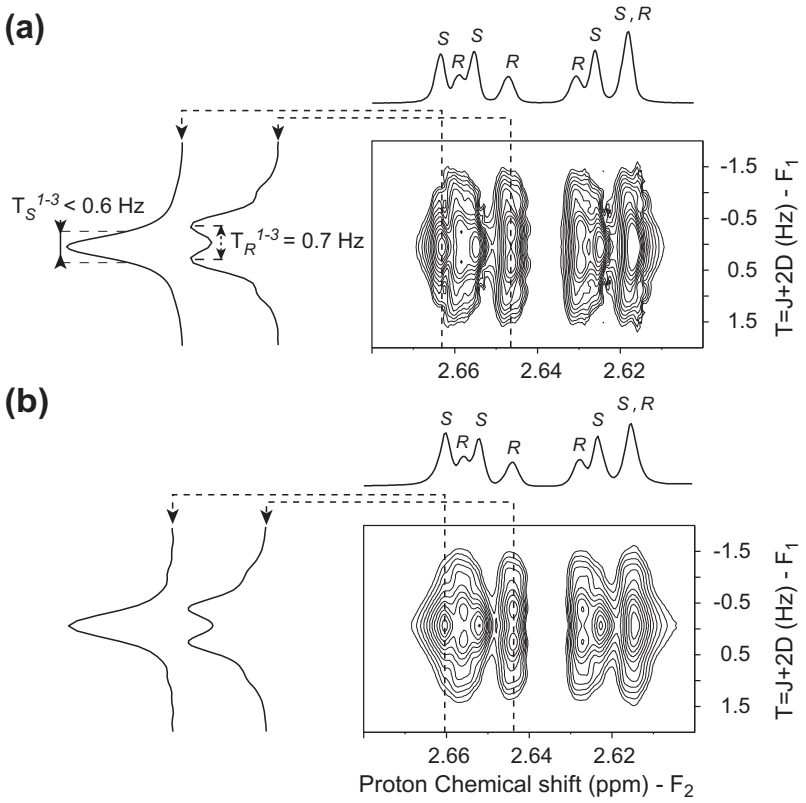

Fig. 7. Enlarged regions from the 2D spectra shown in Fig. 5, which display the correlations centered at H^3 chemical shift, in (a) the G-SERFph and (b) the SERFph experiments. For each spectrum, two columns were extracted in F_1, from lines which can be assigned only to the *S* or *R* enantiomer, and are shown on the left side of the spectra. Note that a small difference in H^3 chemical shift anisotropy between each enantiomer makes the overall multiplet asymmetric in F_2 dimension.

where $\Delta\nu$ is the spectral width which is excited by the semi-selective pulse, γ is the gyromagnetic ratio, G is the gradient pulse strength and l is the sample height detected by the probe. At a very low concentration, a longer experimental time may be needed to record a gradient encoded spectrum.

The duration of a G-SERFph experiment is first and foremost imposed by the minimum number of scans (which we have set to 8 [15]), which is necessary to complete a correct phase cycling. Furthermore, if the spatial frequency sweep which is induced by the pulsed field gradient is adjusted to the width of the spectrum (here 2 ppm), then each signal (whose width can be estimated to 0.1 ppm) is encoded in a cross section which represents 5% of the total sample: the sensitivity of a G-SERFph experiment does not solely depend on the amount of the molecule, but also on the width of its spectrum ! Nevertheless, even in the case of a "standard" spectrum width (about 10 ppm), the sensitivity ratio (1% of the corresponding SERF experiment) will be the same as that of a 2D HSQC ^1H–^{13}C experiment compared to a 1D ^1H spectrum. Moreover, although all the spectra were recorded on a relatively concentrated sample in order to highlight the pulse sequence properties (and notably to study the existence of potentially weak artifacts) within a reasonable experimental time, all the data which were extracted from the G-SERFph experiment (Fig. 5) could have been acquired with a significantly less concentrated sample. Less than 11 h were necessary to record each G-SERFph spectrum, whereas the acquisition of a single SERFph experiment, with a phase cycling which has been limited to four steps, required 7 h. This is due to (i) the restricted spectral width in the indirect dimension (100 Hz), and (ii) the long lifetime of refocused coherences during t_1. Finally, for this sample, the acquisition of the whole set of SERFph spectra which are necessary to collect every coupling involving H^1 spin (*i.e.* one by one) lasted 28 h. This protocol is more than two times longer than a spatial encoding approach which consists in editing every coupling within one –though less sensitive- G-SERFph spectrum.

More generally, for a spin system which is composed of n fully coupled, non-equivalent proton sites, $\frac{n(n-1)}{2}$ SERFph experiments have to be recorded in order to measure every coupling constant. The G-SERFph spectroscopy requires only $(n-1)$ spectra to provide every measurements -and assignments- of the same coupling network. We stress here the potential of gradient encoded selective refocusing spectroscopy as a tool for acquiring more rapidly all the information about large spin networks.

3. Conclusion

In conclusion, we have applied a G-SERFph pulse sequence to the edition of the coupling network in an enantiomeric mixture dissolved in chiral anisotropic solvent. We have demonstrated the quality of the resulting data, which is comparable to what can be obtained using state of the art selective refocusing techniques. The implementation of a spatial frequency encoding in a SERFph pulse sequence provides several potential probes of the enantiomeric discrimination which takes place in the chiral liquid crystalline phase, or in any sample where stereoisomers interact with a chiral agent. We have been able to measure, on a model chiral organic compound, every overall ^1H homonuclear coupling from G-SERFph spectra, and we could run the complete set of experiments faster than with the standard SERFph approach, despite their lower sensitivity.

This application of a frequency sweep to sample spatial encoding, in order to probe specific interactions in separate parts of the sample, paves the way for a generalized strategy for editing NMR

interactions in multi-dimensional experiments: this method is suitable for every structural study where a great number of NMR constraints are required to elucidate -for instance- the differential ordering effect of a given chiral solvent on flexible enantiomers. It should apply to most of the organic compounds whose NMR spectrum (which has to be encoded along the NMR sample) is resolved enough, so that relevant spins nuclei whose couplings are being investigated are *spectrally separated*. In this context, the use of high magnetic fields should contribute to improve the resolution as well as the sensitivity of G-SERFph experiments, and hence facilitate the study of larger molecular systems. We append here that the combination of G-SERF spectroscopy with other techniques that are routinely used to simplify NMR spectra in chiral liquid crystalline solvents, such as Variable Angle Sample Spinning (VASS[29,36]), should allow to apply this approach to molecular systems where dipolar couplings have to be scaled down, in order to produce first-order spectra.

Acknowledgment

The authors thank Prof. James. W. Emsley for helpful discussions.

Appendix A. Supplementary data

The *J*-resolved spectrum recorded on the propylene oxide sample that is studied in this paper (Fig. S1). The G-SERFph proton 2D spectra which were acquired for the edition of the coupling networks around H^3 (Fig. S2a) and H^4 (Fig. S2b) proton spins, respectively. The sums of the columns from the four G-SERFph spectra which were recorded for the edition of the coupling networks (Fig. S3). A table displaying the overall homonuclear proton couplings ($T = J + 2D$) in the propylene oxide sample which is studied in this paper (Table 1). Supplementary data associated with this article can be found, in the online version, at doi:10.1016/j.jmr.2011.01.030.

References

[1] L. Frydman, A. Lupulescu, T. Scherf, Principles and features of single-scan two-dimensional NMR spectroscopy, J. Am. Chem. Soc. 125 (2003) 9204–9217.
[2] M.J. Thrippleton, J. Keeler, Elimination of zero-quantum interference in two-dimensional NMR spectra, Angew. Chem., Int. Ed. 42 (2003) 3938–3941.
[3] P. Pelupessy, Adiabatic single scan two-dimensional NMR spectrocopy, J. Am. Chem. Soc. 125 (2003) 12345–12350.
[4] A.J. Pell, R.A.E. Edden, J. Keeler, Broadband proton-decoupled proton spectra, Magn. Reson. Chem. 45 (2007) 296–316.
[5] D.J. Peterson, N.M. Loening, QQ-HSQC: a quick, quantitative heteronuclear correlation experiment for NMR spectroscopy., Magn. Reson. Chem. 45 (2007) 937–941.
[6] Y. Shrot, L. Frydman, Spatial encoding strategies for ultrafast multidimensional nuclear magnetic resonance, J. Chem. Phys. 128 (2008).
[7] P. Pelupessy, L. Duma, G. Bodenhausen, Improving resolution in single-scan 2D spectroscopy, J. Magn. Reson. 194 (2008) 169–174.
[8] M. Gal, T. Kern, P. Schanda, L. Frydman, B. Brutscher, An improved ultrafast 2D NMR experiment: Towards atom-resolved real-time studies of protein kinetics at multi-Hz rates, J. Biomol. NMR 43 (2009) 1–10.
[9] G. Morris, J. Aguilar, R. Evans, S. Haiber, M. Nilsson, True chemical shift correlation maps: A TOCSY experiment with pure shifts in both dimensions, J. Am. Chem. Soc. 132 (2010) 12770–12772.
[10] A.J. Pell, J. Keeler, Two-dimensional J-spectra with absorption-mode lineshapes, J. Magn. Reson. 189 (2007) 293–299.
[11] R. Freeman, E. Kupce, New methods for fast multidimensional NMR, J. Biomol. NMR 27 (2003) 101–113.
[12] E. Kupce, R. Freeman, B.K. John, Parallel acquisition of two-dimensional NMR spectra of several nuclear species, J. Am. Chem. Soc. 128 (2006) 9606–9607.
[13] R.R. Ernst, G. Bodenhausen, A. Wokaun, Principles of Nuclear Magnetic Resonance in One and Two Dimensions, Clarendon Press, Oxford, 1987.
[14] N. Giraud, M. Joos, J. Courtieu, D. Merlet, Application of a ^{1}H delta-resolved 2D NMR experiment to the visualization of enantiomers in chiral environment, using sample spatial encoding and selective echoes., Magn. Reson. Chem. 47 (2009) 300–306.
[15] N. Giraud, L. Beguin, J. Courtieu, D. Merlet, Nuclear magnetic resonance using a spatial frequency encoding: application to J-Edited spectroscopy along the sample, Angew. Chem., Int. Ed. 49 (2010) 3481–3484.
[16] I. Canet, J. Courtieu, A. Loewenstein, A. Meddour, J.M. Pechine, Enantiomeric analysis in a polypeptide lyotropic liquid-crystal by deuterium NMR, J. Am. Chem. Soc. 117 (1995) 6520–6526.
[17] R.Y. Dong, Nuclear Magnetic Resonance of Liquid Crystals (Partially Ordered Systems), Springer-Verlag, 1994.
[18] J.W. Emsley, Nuclear Magnetic Resonance of Liquid Crystals, Springer, 1985.
[19] P. Lesot, Y. Gounelle, D. Merlet, A. Loewenstein, J. Courtieu, Measurement and analysis of the molecular ordering tensors of 2 enantiomers oriented in a polypeptide liquid-crystalline system, J. Phys. Chem. 99 (1995) 14871–14875.
[20] P. Lesot, D. Merlet, J. Courtieu, J.W. Emsley, T.T. Rantala, J. Jokisaari, Calculation of the molecular ordering parameters of (±)-3-butyn-2-ol dissolved in an organic solution of poly(gamma-benzyl-L-glutamate), J. Phys. Chem. A 101 (1997) 5719–5724.
[21] C. Aroulanda, M. Sarfati, J. Courtieu, P. Lesot, Investigation of the enantioselectivity of three polypeptide liquid-crystalline solvents using NMR spectroscopy, Enantiomer 6 (2001) 281–287.
[22] K. Kobzar, H. Kessler, B. Luy, Stretched gelatin gels as chiral alignment media for the discrimination of enantiomers by NMR spectroscopy, Angew. Chem., Int. Ed. 44 (2005) 3145–3147.
[23] G. Kummerlowe, M.U. Kiran, B. Luy, Covalently Cross-linked Gelatin Allows Chiral Distinction at Elevated Temperatures and in DMSO, Chem.– Eur. J. 15 (2009) 12192–12195.
[24] J. Farjon, J.P. Baltaze, P. Lesot, D. Merlet, J. Courtieu, Heteronuclear selective refocusing 2D NMR experiments for the spectral analysis of enantiomers in chiral oriented solvents, Magn. Reson. Chem. 42 (2004) 594–599.
[25] B. Baishya, U. Ramesh Prabhu, N. Suryaprakash, A.W. Graham, Analyses of Proton NMR Spectra of Strongly and Weakly Dipolar Coupled Spins: Special Emphasis on Spectral Simplification, Chiral Discrimination, and Discerning of Degenerate Transitions, Annual Reports on NMR Spectroscopy, Academic Press, 2009, pp. 331–423.
[26] N. Nath, N. Suryaprakash, Enantiodiscrimination and extraction of short and long range homo- and hetero-nuclear residual dipolar couplings by a spin selective correlation experiment, Chem. Phys. Lett. 496 (2010) 175–182.
[27] N. Nath, N. Suryaprakash, Selective detection of single-enantiomer spectrum of chiral molecules aligned in the polypeptide liquid crystalline solvent: Transition selective one-dimensional H-1–H-1 COSY, J. Magn. Reson. 202 (2010) 34–37.
[28] U.R. Prabhu, N. Suryaprakash, Selective homonuclear decoupling in H-1 NMR: application to visualization of enantiomers in chiral aligning medium and simplified analyses of spectra in isotropic solutions, J. Phys. Chem. A 114 (2010) 5551–5557.
[29] L. Beguin, J. Courtieu, L. Ziani, D. Merlet, Simplification of the H-1 NMR spectra of enantiomers dissolved in chiral liquid crystals, combining variable angle sample spinning and selective refocusing experiments, Magn. Reson. Chem. 44 (2006) 1096–1101.
[30] L. Beguin, N. Giraud, J.M. Ouvrard, J. Courtieu, D. Merlet, Improvements to selective refocusing phased (SERFph) experiments, J. Magn. Reson. 199 (2009) 41–47.
[31] M. Sarfati, P. Lesot, D. Merlet, J. Courtieu, Theoretical and experimental aspects of enantiomeric differentiation using natural abundance multinuclear NMR spectroscopy in chiral polypeptide liquid crystals, Chem. Commun. 10 (2000) 2069–2081.
[32] R. Freeman, High-resolution NMR using selective excitation, J. Mol. Struct. 266 (1992) 39–51.
[33] W.P. Aue, J. Karhan, R.R. Ernst, Homonuclear broad band decoupling and two-dimensional J-resolved NMR spectroscopy, J. Chem. Phys. 64 (1976) 4226–4227.
[34] J. Emsley, J. Lindon, NMR spectroscopy using liquid crystal solvents, Pergamon Press, Oxford, 1975.
[35] M.J. Thrippleton, R.A.E. Edden, J. Keeler, Suppression of strong coupling artefacts in J-spectra, J. Magn. Reson. 174 (2005) 97–109.
[36] J. Courtieu, J.P. Bayle, B.M. Fung, Variable-angle sample-spinning NMR in liquid-crystals, Prog. NMR Spectrosc. 26 (1994) 141–169.